Journal of Structural Geology, Vol. 15, Nos 3–5, pp. 451 to 464, 1993
Printed in Great Britain

0191-8141/93 $06.00+0.00

Strain variations and three-dimensional strain factorization at the transition from the southern to the central Appalachians

B. A. COUZENS and W. M. DUNNE

Department of Geological Sciences, University of Tennessee, Knoxville, TN 37996, U.S.A.

and

C. M. ONASCH and R. GLASS

Department of Geology, Bowling Green State University, Bowling Green, OH 43403, U.S.A.

(*Received* 23 *December* 1991; *accepted in revised form* 31 *August* 1992)

Abstract—The transition between the southern and the central Appalachian foreland thrust system is a region subjected to at least two non-coaxial deformations, where typical two-dimensional analyses such as cross-section balancing or plane-strain retro-deformation cannot be applied. Three-dimensional factorization can simulate the non-coaxial strain history. Simulation results for compaction and layer-parallel shortening (LPS) were compared to finite strains of 16 quartz arenite samples from the Tuscarora Sandstone. Successful simulations indicate: in the southern Appalachians—30–35% total compaction by volume loss including a 4.5–9% E–W horizontal shortening during lithification, and 5% LPS along 150–330° by plane strain or axial symmetric flattening; in the central Appalachians—30–35% total compaction by volume loss including a 3–7% N–S horizontal shortening during lithification, and 10% LPS along 120–300° by plane strain or axial symmetric flattening; in the transition zone—30% compaction by volume loss including a 3% E–W horizontal shortening during lithification, 5% 'southern' LPS along 150–330° by axial symmetric flattening, and 5–10% 'central' shortening along 130° or 140° by plane strain or axial symmetric flattening at 10° to the normal 'central' trend. From the simulations, horizontal shortening in the southern Appalachians during lithification in the Mississippian was greater than the later Alleghanian deformation. This shortening probably represents a very early LPS developed in unlithified sand that required less deviatoric stress to deform than did the cemented quartz arenites during later tectonic deformation. Also, the oblique and weaker central tectonic LPS in the transition zone probably represents behavior at the limits of central Appalachian deformation. Finally, the LPS simulations indicate that axial symmetric flattening (oblate strain) is more successful than plane strain as the representative behavior, so caution is recommended in assuming plane strain as the dominant strain behavior in orogenic forelands.

INTRODUCTION

A KEY aspect to the structural analysis of a region is assessing the role of internal strain during deformation. A number of recent studies have attempted to quantify the role of strain in two dimensions. Two approaches have been used: backwards modeling that retro-deforms or unstrains the rocks (Cobbold 1979, Hossack 1979) and forward modeling for a series of strain events to create the observed strains (Ramsay & Huber 1983, Kligfield *et al.* 1984). Retro-deformation has commonly been done where plane strain in the plane perpendicular to tectonic strike and parallel to regional displacements exists or is assumed. Strain integration has been used to remove finite strain to produce an undeformed state (Reks & Gray 1983, Woodward *et al.* 1986, Gray & Willman 1991). Even in cases in which three-dimensional strain data have been collected, retro-deformation has only been attempted in two dimensions (Protzman & Mitra 1990).

Forward modeling, or strain factorization (Ramsay & Huber 1987, p.596), simulates a rock deforming through a series of events to yield a calculated finite strain that can be compared to measured strains. The choice and sequence of events is constrained by the types of deformation in the region, the types of meso- and microstructures present, and their cross-cutting relationships. Factorization is performed by multiplying a series of matrices, each of which represents a strain or deformation increment (Ramsay 1967, p.322, Kligfield *et al.* 1984, Ramsay & Huber 1987, p.596). The resultant deformation matrix is used to calculate the magnitude and orientation of the finite strain ellipsoid. This approach has also been used in two dimensions to model plane strain parallel to transport (Evans & Dunne 1991).

Strain factorization in three dimensions has been described (Ramsay 1967, p.326, Means 1976), however, to the authors' knowledge, it has not been applied to real data. Although factorization in two dimensions is significantly easier to calculate than in three dimensions, it is limiting because all the deformation must take place in the same reference plane. Three-dimensional factorization eliminates this restriction and allows the simulation of non-coaxial deformations such as: (1) overlapping deformation between two non-parallel tectonic belts; (2) sequential non-coaxial strain events; and (3) tectonic modification of pretectonic strains from lithification. Three-dimensional factorization also more completely

represents three-dimensional strain events such as axial symmetric flattening (oblate strain) or stretching (prolate strain), even though they may be modeled in two dimensions.

The purpose of this paper is to apply three-dimensional strain factorization to finite strain data from two adjacent foreland thrust systems and the transition between them. Factorization will quantify the sequential strains in each system and describe their non-coaxial interactions in the transition zone.

REGIONAL GEOLOGY

The study area is located across the transition from the southern to the central Appalachian foreland thrust system. The southern Appalachians have a regional strike of 060°, the central Appalachians have a regional strike of 030°, and the transition between the two has an intermediate strike of about 050° (Fig. 1). The change in trend is the result both of an irregularly shaped continental margin before collision and of a two-stage deformation history in which southern structures initiated prior to deformation in the central Appalachians (Geiser & Engelder 1983, Dean *et al.* 1988, Hatcher *et al.* 1989). Structural style also changes from thrust-dominated in the southern system to macrofold-dominated in the roof sequence above the central Appalachians blind thrust system (Fig. 1). This change in style results mainly from northward thickening of Middle Ordovician and Middle Devonian shales (Colton 1970, Rader & Henika 1978, Bartholomew 1987, Kreisa & Springer 1987) that serve as additional décollements for roof faults in the thrust system.

Strain data were measured from the Lower Silurian Tuscarora Sandstone, a medium- to fine-grained quartz arenite of uniform composition and no open porosity. This unit was chosen because: (1) it is probably the best exposed unit in the area (Dennison 1970, Whisonant 1977); (2) it is present in a variety of structural positions in both the thrust system and the roof sequence; (3) it has a framework-supported texture (Hayes 1974) that is well suited to spatial strain techniques such as the normalized Fry method (Erslev 1988); and (4) strain-sensitive lithologies such as grainstones (Groshong 1972, 1988, Rutter 1976) were unavailable across the region because of facies changes and poor exposures.

Deformation within the Tuscarora Sandstone is partitioned between discontinuous structures such as meso- and microfractures, cataclastic bands, and transgranular solution surfaces that are heterogeneously distributed, and grain-scale structures such as undulatory or patchy extinction, deformation lamellae, deformation bands and grain-to-grain solution surfaces which are homogeneously distributed (Onasch & Dunne 1993). Finite strains measured in this study record deformations from the homogeneously distributed microstructures and not the heterogeneous distributed strains from structural discontinuities.

METHODOLOGY

Samples from seven strike-perpendicular traverses were cut into three mutually perpendicular thin-sections: bed-parallel, bed-normal along strike, and bed-normal along dip (see Appendix 1). Cathodoluminescence photomicrographs were taken of each thin-section and used for strain measurement because the luminescence distinguishes detrital grains from their optically continuous cement overgrowths. Use of detrital quartz grains as markers yields original grain centers, preventing errors that can result from the use of grain centers from transmitted light images where the visible

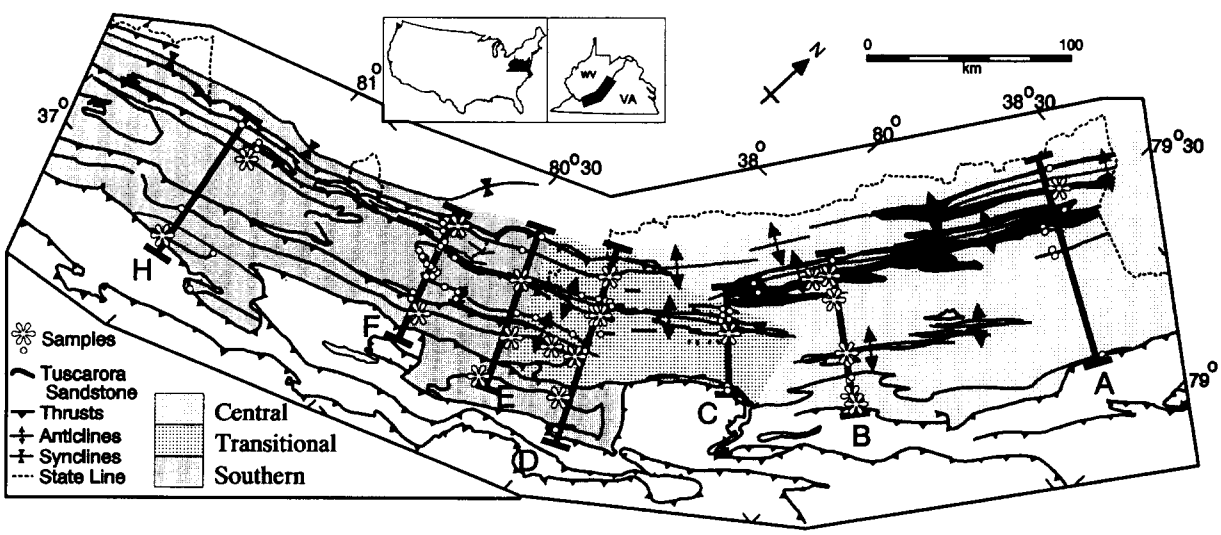

Fig. 1. Map of distribution of major faults, major folds, and the outcrop of the Tuscarora Sandstone across the transition from the southern to the central Appalachian foreland. Single capital letters designate sample lines (bold straight lines). Sample sites considered in the study are white asterices, other sample sites are white dots. The transition zone bounds the region where macrostructures have an intermediate strike of between 030° and 060° (Rodgers 1970, Dean *et al.* 1988).

grains include the optically continuous cement (Dunne *et al.* 1990). Also, the original centers record compaction during lithification as well as tectonic strains. The shapes and positions of 200 quartz grains were digitized in each section and strain determined by applying the normalized Fry method (Fry 1979, Erslev 1988). Strain ellipsoids were then calculated from the three mutually perpendicular ellipses for each sample using the TRIAX program (Gendzwill & Stauffer 1981).

OBSERVED FINITE STRAINS

X/Y, Y/Z and X/Z ratios vary between 1.01 and 1.80 with means and standard deviations of 1.15 ± 0.08, 1.18 ± 0.09 and 1.35 ± 0.11, respectively (see Appendix 1). Ellipsoid shapes vary considerably and do not yield a simple pattern. For example, a Flinn plot of the data (Fig. 2) shows considerable scatter with no separation for samples from the southern, central and transition regions (Fig. 1). The relationship between the abundances of microstructures and strain magnitude was tested by linear regression. The correlation between finite strain magnitude and abundance of each microstructure (undulatory extinction, patchy extinction, deformation lamellae, deformation bands, pressure solution surfaces, fluid inclusion planes, microveins and cataclastic bands) ranged between −0.115 and 0.086. The critical r-value with a 95% confidence limit, as determined by a t-test, is 0.225. Therefore, finite strain does not correlate with microstructural development.

The apparent lack of correlation between finite strain magnitude and regional position or microstructural abundance is partially explained by the geometry of the finite strain ellipsoids. When bedding for all samples is restored to the horizontal to provide a common reference frame for comparison of strain-axes orientations

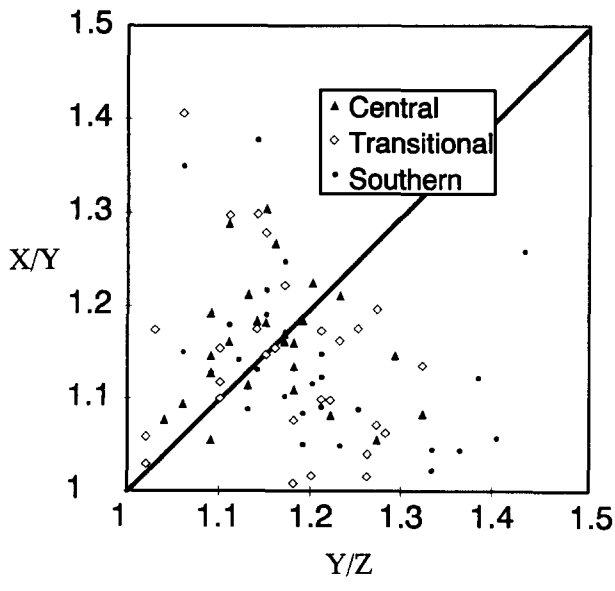

Fig. 2. Flinn plot of all strain data by region.

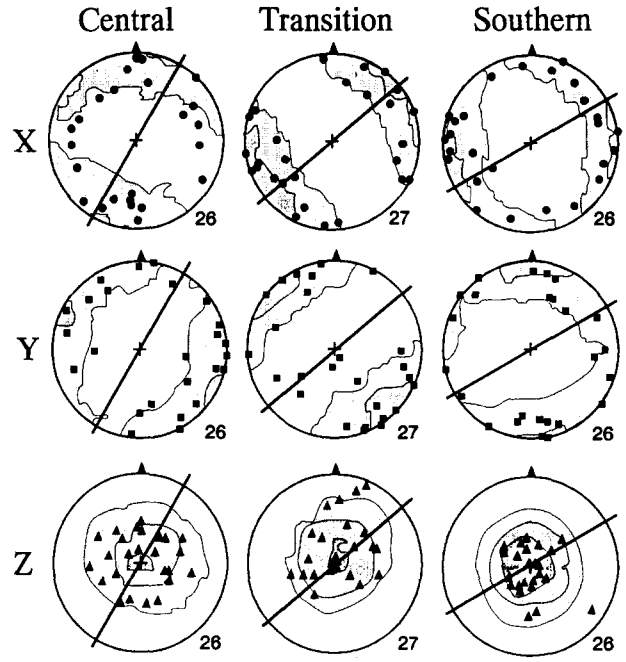

Fig. 3. Equal-area lower-hemisphere projections depicting strain-ellipsoid axial orientations ($X \geq Y \geq Z$). Bedding is restored to the horizontal to provide a common reference frame. The data were contoured using the Kamb (1959) method with a 3σ contour interval. For 26 or 27 poles, the counting area is about 25% of the projections' total area. For a 95% (3σ) confidence level that a point concentration is non-random, greater than 6.7 poles must be found in the counting area. The black line across each net is parallel to regional strike.

(Fig. 3), the most notable feature is that the Z-axes of the strain ellipsoids show a strong bedding-normal orientation. The pervasiveness of this geometry in all structural positions and tectonic regions suggests that diagenetic compaction is the dominant strain in the Tuscarora Sandstone.

The silica-cemented quartz arenites of the Tuscarora Sandstone, which lack open porosity (Sibley & Blatt 1976, Houseknecht 1988, and unpublished data) are derived from well sorted quartz sands (Cotter 1988). Similar Holocene sands have original porosities of about 40% (Beard & Weyl 1973, Pryor 1973) and diagenetic studies of cementation in the Tuscarora Sandstone indicate a similar original porosity (Houseknecht 1988). Therefore, we assume that the Tuscarora Sandstone had an original porosity of 40% for subsequent calculations about compaction in the deformation models. During lithification, original porosity was either: (1) physically destroyed by grain-boundary sliding, grain cataclasis and grain-to-grain solution causing a volume loss; or (2) chemically preserved by infilling of optically continuous overgrowths of silica (Heald 1955, 1956, Sibley & Blatt 1976, Mitra & Beard 1980, Houseknecht 1987, 1988, Stephenson *et al.* 1991, Elias & Hajash 1992). The relative role of these physical and chemical processes was determined by point-counting 200 points for framework grains vs cement. 10 ± 5% of all bed-normal, dip-parallel sections were composed of cement and 11 ± 5% of all bed-parallel sections were composed of cement. Consequently, assuming 40% original porosity, approximately three quarters of the porosity was physi-

cally destroyed during lithification, causing a 30 ± 5% volume loss in the Tuscarora Sandstone. This physical destruction is manifested in the sandstone fabric by a limited number of fractured grains (F, Fig. 4), interpenetrated grains including sutured contacts (P, Fig. 4), and rare weakly luminescent silica cement (Fig. 4). This volume loss must be greater than the magnitude of any bedding-parallel tectonic shortening because the Z-axes of strain ellipsoids are sub-normal to bedding.

Tectonic microstructures such as deformation lamellae, deformation bands, fluid inclusion planes and microveins affect both detrital grains and their cement (Onasch & Dunne 1993). The effects of this tectonic deformation are visible in the stereonets (Fig. 3) as groupings of X- and Y-axes in the bedding-plane into weak (south and central) and strong (transition) polar concentrations. For the weak polar concentrations, about 50% of the X-axes are N–S-trending in the central Appalachians and E–W-trending in the southern Appalachians as opposed to only 10–20% being parallel to strike. Similarly for the Y-axes, about 30% are E–W-trending in the central Appalachians and 50% are N–S-trending in the southern Appalachians whereas only 10–15% are normal to regional strike. These concentrations represent a modification to a simple bedding-plane girdle expected for uniaxial vertical compaction during lithification.

The polar concentrations from tectonic deformation are strongest in the transition zone where two tectonic deformations have occurred (Dean *et al.* 1988), and the greatest abundance of microstructures are developed (Onasch & Dunne 1993). Yet, even in this region, tectonic strains have been insufficient to exceed the 30% compaction volume loss, because the Z-axes are still sub-normal to bedding. The polar concentrations of X- and Y-axes are slightly oblique to regional strike and dip with greatest obliquity in the southern Appalachians and least in the transition zone.

Because diagenetic compactional strains dominate, the effects of tectonic strains are difficult to determine qualitatively from the finite strain data. Consequently, strain factorization was applied to the finite strains to verify which proposed sequences of incremental strain magnitudes and orientations would yield the measured strains.

STRAIN FACTORIZATION OF REGIONAL EVENTS

Before factorization, a co-ordinate system must be defined. The chosen system in the deformed state has z vertical, y strike-parallel and x strike-perpendicular (dip-parallel) and the equivalent system in the undeformed state is ZYX, respectively, in terms of a deformation matrix:

$$\begin{bmatrix} \frac{\delta x}{\delta X} & \frac{\delta x}{\delta Y} & \frac{\delta x}{\delta Z} \end{bmatrix}$$

$$D = \begin{vmatrix} \frac{\delta y}{\delta X} & \frac{\delta y}{\delta Y} & \frac{\delta y}{\delta Z} \\ \frac{\delta z}{\delta X} & \frac{\delta z}{\delta Y} & \frac{\delta z}{\delta Z} \end{vmatrix},$$

which is used to map points in a volume from original positions to strained positions (Ramsay 1967, Means 1976, p. 178, Kligfield *et al.* 1984, Ramsay & Huber 1987).

Based on observed microstructures and strain histories from this and other studies in the Appalachians, several strain events may have affected the Tuscarora Sandstone. (1) A compaction strain with volume loss of about 30% ($-\Delta$) in the z-direction (vertical) is inferred from grain-to-grain truncations, a lack of porosity, and the presence of only a limited amount of cement (Sibley & Blatt 1976, Houseknecht 1988)(Table 1a). (2) A tectonic layer-parallel shortening (LPS) by intragranular deformation is recorded by undulatory and patchy extinction, deformation lamellae and deformation bands (Onasch & Dunne 1993). LPS commonly precedes macrofolding or thrusting (Marshak & Engelder 1985, Mitra & Yonkee 1985, Geiser 1988), is typically between 5 and 15% in the Appalachians, and here is treated as either a plane strain or an axial symmetric flattening (Table 1b & c). (3) A rigid rotation of bedding may have occurred by macrofolding or emplacement over a thrust ramp (Table 1d). (4) A layer-normal shortening event (causing dip-parallel extension) for beds rotated into steep dips in northwest anticline limbs, footwall ramps and hangingwall ramps (Berger *et al.* 1979, Dunne 1986, Onasch 1990), is recorded by bed-normal, strike-parallel microfractures, meso-scale contraction faults and bed-parallel stylolites (Onasch & Dunne 1993)(Table 1e). Any of the above events may be applied obliquely in the co-ordinate system using the relationship: $E = C^{-1}MC$, where E is the deformation in the chosen co-ordinate system (xyz), M is the deformation matrix at an angle, θ, to the co-ordinate system and C describes the rotation between the axes of the co-ordinate system and the axes of the event (Table 1) (Boas 1983).

Because matrix multiplication is not commutative (Anton 1984), superposition of the youngest strain (deformation matrix E_3) on the intermediate strain event (deformation matrix E_2) that was previously superimposed on the oldest strain event (deformation matrix E_1), yields a resultant deformation, D, of:

$$D = E_3E_2E_1.$$

The strain ellipsoid shape and orientation may be conveniently calculated from the deformation matrix D (see Appendix 2), using commercially available spreadsheets.

Two regional strain events have been chosen for simulation to investigate their interactions across the transition zone in the Appalachians: (1) a diagenetic compaction modeled entirely as a volume loss; and (2) a LPS event with no volume loss. The latter was chosen because the Tuscarora Sandstone lacks microstructural

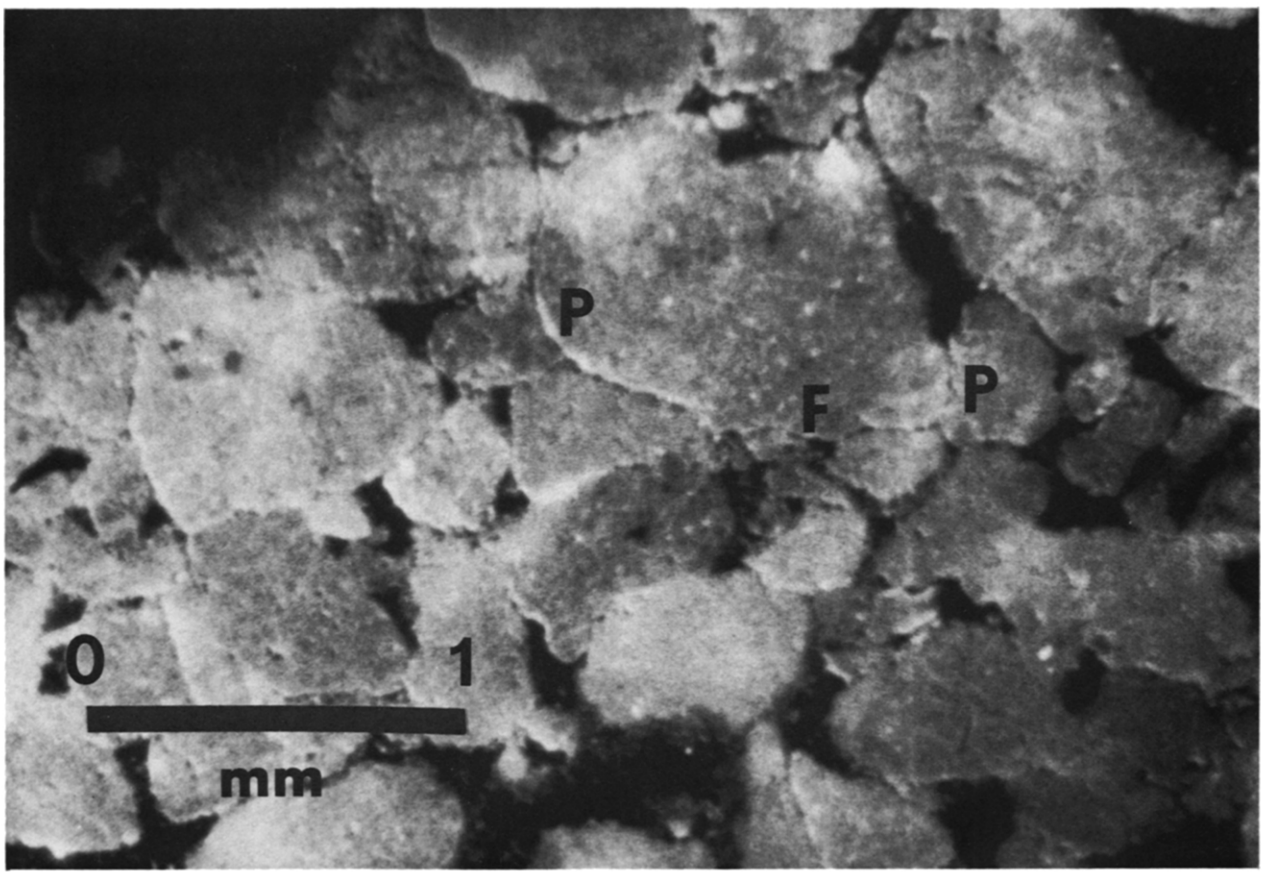

Fig. 4. Cathodoluminescent photomicrograph of the Tuscarora Sandstone in the transport plane showing compactional fabric elements. Bedding is parallel to the scale bar. P—interpenetrated and sutured grain contacts; F—fractured grain.

evidence for solution during LPS, such as transgranular, bed-normal solution structures. The LPS was separately modeled as plane strain and axial symmetric flattening.

Samples were chosen to provide a comparison with the results of the factorizations using the following constraints: (1) location in either SE-dipping hanging-wall flats or macro-anticline limbs that record only compaction and LPS in their microstructural suites (Onasch & Dunne 1993); (2) location in either the central or southern regions where only one layer-parallel shortening event has occurred (Geiser & Engelder 1983, Dean *et al.* 1988); and (3) orientation of *Z*-axes sub-normal to bedding to preclude the presence of other local strains. Twelve of the 15 possible samples (white asterices in the central and southern Appalachians, Fig 1; see Appendix 1) met these criteria (Table 2).

Simple two-event simulations

Compaction (varied from 10 to 35% in 5% increments) entirely by volume loss, followed by LPS (varied from 5 to 15% in 5% increments) as either plane strain or axial symmetric flattening was modeled as a two-event sequence, yielding a total of 36 simulations. The simulations do not include LPS by volume loss as the microstructures in the sandstone lack post-compactional solution structures.

When plotted on a Flinn plot (Fig. 5a), three simulations lie within the field defined by one standard deviation about the means for *X*/*Y* and *Y*/*Z* ratios from the central Appalachians (Table 2), implying that three acceptable deformation paths exist from the two-event histories. When the same simulations are plotted in *Y*/*Z*:*X*/*Z* space (Fig. 5b), only one of the three simulations lies within the field for the central Appalachian data. It has the only *X*/*Z* ratio within 1 SD of the mean *X*/*Z* ratio, implying that only one acceptable deformation path exists. Consequently, using only a Flinn plot to compare results with actual data does not sufficiently constrain the simulations, and the use of both plots is necessary to determine which simulations successfully fit the data. This approach was used throughout the subsequent modeling. The successful simulation for the data of the central Appalachians has 25% compaction with 10% LPS by axial symmetric flattening.

In the southern region, a total of six simulations lie within the field defined by one standard deviation about the means for *X*/*Y* and *Y*/*Z* ratios (Fig. 5a). On the *Y*/*Z*:*X*/*Z* plot, only four of those simulations lie within the field for the southern Appalachians (Fig. 5b). The four simulations represent: 10% compaction with 15% LPS by axial flattening; 25% compaction with 5 or 10% LPS by axial flattening; and 30% compaction with 10% LPS by plane strain. All simulations are consistent with the measured amount of cement (10 ± 5%) and the inferred compactions of 30 ± 5%.

The deformation paths for admissible simulations of both the central and southern Appalachians are plotted on logarithmic Flinn plots (Fig. 6a), which better illustrate small strains and display constant deformation paths as straight lines (Ramsay 1967, p.329, Ramsay & Wood 1973). Although the strain paths move to the right along the *Y*/*Z* axis, they do not enter the true flattening field because a pre-tectonic volume loss moves the plane-strain line off of the $k = 1$ line to the right an equivalent amount (Ramsay & Wood 1973). Consequently, the subsequent LPS moves the accumulated strain into the true constrictional field.

An inconsistency is built into all of these simulations because they only represent strain events that are parallel to the axes of the co-ordinate system. As such, they yield *X* and *Y* axes that are parallel to strike and dip (the co-ordinate system), respectively. Yet, the orientation of the real axes (Fig. 3) are oblique, particularly in the southern Appalachians. So, while these models correctly predict strain magnitudes, they do not predict axial orientations.

Simulations with triaxial sedimentary compaction

A strain that is not parallel to the co-ordinate system and is non-coaxial with other strains must occur to obtain *X*- and *Y*-axes that are oblique to regional strike. As this strain is non-coaxial and not in the regional tectonic transport plane, a three-dimensional simulation must be used. Because the samples have been selected to include only microstructures related to compaction and LPS, one of the two events must be non-coaxial. Generally, LPS is parallel to regional transport. Specifically, in the Appalachians where investigations have been able to partition the LPS increment, it has been shown to be transport-parallel and perpendicular to regional strike (Engelder & Geiser 1979, Nickelsen 1979, Simon & Gray 1982, Geiser & Engelder 1983, Evans & Dunne 1991). Consequently, compaction must be the non-coaxial event.

Most studies treat compaction as a uniaxial loading event with negligible horizontal deviatoric stress (e.g. Narr & Currie 1982); however, tectonic torques from plate boundaries generate horizontal deviatoric stresses thousands of kilometers from the boundary (Zoback & Zoback 1990). The Tuscarora Sandstone in the southern and central Appalachians was probably near an active plate boundary (Geiser & Engelder 1983, Hatcher *et al.* 1989) and reached burial depths for lithification when that boundary was active (Geiser & Engelder 1983, Ferrill & Thomas 1988). In the central Appalachians, rapid accumulation of Acadian foreland sediments (Colton 1970, Meckel 1970) buried the Tuscarora Sandstone to sufficient depth for lithification by the Middle Devonian. Maximum horizontal compression was then oriented approximately E–W (present-day co-ordinates) across the region (Ferrill & Thomas 1988). Thus, an E–W horizontal component of shortening by porosity loss, oblique to the present regional strike, was included in the central Appalachian compaction event.

Three-dimensional models were run to simulate 25–35% compaction with a percentage of horizontal volume loss (5–30% of the total volume loss during compac-

tion), followed by LPS plane strain or axial symmetric flattening without volume loss as indicated by the microstructures. Sixty-eight of 108 total simulations yielded trends of X-axes within the necessary range of 020–030° (Table 2). Of those, four lie within the field defined by one standard deviation about the means for X/Y and Y/Z ratios (Fig. 5c). On the Y/Z:X/Z plot, only three of those simulations lie within the field for the central Appalachians (Fig. 5d and Table 3).

The Tuscarora Sandstone in the southern, in contrast to the central, Appalachians was not buried under the Acadian molasse during the Devonian. Instead, it was buried to lithification depths during the Mississippian by foreland sediments related to the onset of Alleghanian deformation from the south (Geiser & Engelder 1983, Hatcher *et al.* 1989). This early deformation was driven by an approximately N–S-trending orogenic compression, which was simulated in the factorization by a N–S component of horizontal shortening by volume loss during compaction.

Forty simulations for the southern Appalachians, of a total of 108 as in the central Appalachians, yielded X-axes trending similar to the observed ranges of 070–080° (Table 2). Of these, 10 lie within the field defined by 1 SD about the means for X/Y and Y/Z ratios (Fig. 5c). On the Y/Z:X/Z plot, all 10 simulations lie within the field for the southern Appalachians (Fig. 5d and Table 3). The results of the simulations show that horizontal shortening during compaction was larger in the southern than the central Appalachians, which is consistent with the closer proximity of the southern Appalachians to a source of orogenic compression at the time of lithification (Geiser & Engelder 1983, Ferrill & Thomas 1988, Hatcher *et al.* 1989).

The deformation paths for the 13 admissible simulations (Fig. 6b) move to the right along the Y/Z axis and lift off the Y/Z axis because there is now a volume loss in the horizontal (XY plane). Simulations with larger amounts of horizontal volume loss during compaction have paths at larger angles to the Y/Z axis. Even though the paths are not along the Y/Z axis, they still do not plot in the true flattening field, because the pre-tectonic volume loss moves the plane-strain line off the $k = 1$ line to the right (Ramsay & Wood 1973). As a result, the subsequent LPS in these simulations moves the strain paths into the true constrictional field.

An interesting result of the strain factorization in the southern Appalachians is that horizontal shortening during compaction would appear to be greater than the shortening during Alleghanian LPS after lithification. Three points support this result: (1) quartz sand aggregates have greater differential stresses at grain contacts,

Table 1. Matrices for possible strains in the Tuscarora Sandstone

	Deformation	Deformation matrix
a.	Compaction Δ = volume loss	$E = \begin{bmatrix} 1 & 0 & 0 \\ 0 & 1 & 0 \\ 0 & 0 & 1+\Delta \end{bmatrix}$
b.	Plane strain LPS α = engineering strain (percent shortening = $-\alpha$)	$E = \begin{bmatrix} 1+\alpha & 0 & 0 \\ 0 & 1 & 0 \\ 0 & 0 & (1+\alpha)^{-1} \end{bmatrix}$
c.	Axial symmetric LPS α = engineering strain (percent shortening = $-\alpha$)	$E = \begin{bmatrix} 1+\alpha & 0 & 0 \\ 0 & (1+\alpha)^{-1/2} & 0 \\ 0 & 0 & (1+\alpha)^{-1/2} \end{bmatrix}$
d.	Rigid-body rotation θ degrees in xz plane	$E = \begin{bmatrix} \cos\theta & 0 & -\sin\theta \\ 0 & 1 & 0 \\ \sin\theta & 0 & \cos\theta \end{bmatrix}$
e.	Layer-normal shortening α = engineering strain (percent shortening = $-\alpha$)	$E = \begin{bmatrix} (1+\alpha)^{-1} & 0 & 0 \\ 0 & 1 & 0 \\ 0 & 0 & 1+\alpha \end{bmatrix}$
f.	Plane strain LPS at θ° to co-ordinate system	$M = \begin{bmatrix} 1+\alpha & 0 & 0 \\ 0 & 1 & 0 \\ 0 & 0 & (1+\alpha)^{-1} \end{bmatrix}$ $C = \begin{bmatrix} \cos\theta & -\sin\theta & 0 \\ \sin\theta & \cos\theta & 0 \\ 0 & 0 & 1 \end{bmatrix}$ where* $E = C^{-1}MC$

*Note that $E \neq M$ because matrix multiplication is not commutative.

Table 2. Finite strain information for samples in SE-dipping hangingwall flats and macro-anticlinal fold limbs with the Z axis subnormal to bedding

Region	Average X/Y	Average Y/Z	Average X/Z	X axis trend
Central (6)	1.18 ± 0.08	1.16 ± 0.03	1.38 ± 0.09	020–030°
Southern (6)	1.13 ± 0.07	1.18 ± 0.06	1.33 ± 0.08	070–080°
Transition (4)	1.15 ± 0.13	1.18 ± 0.06	1.36 ± 0.09	040–050°

See Appendix 1 for details of stations: (1) central—A8, B2, B3, B9, B10, MM2; (2) southern—D9, E8, F15, H2, SC4, SC6; (3) transition—C3, D6a, E5, E7.

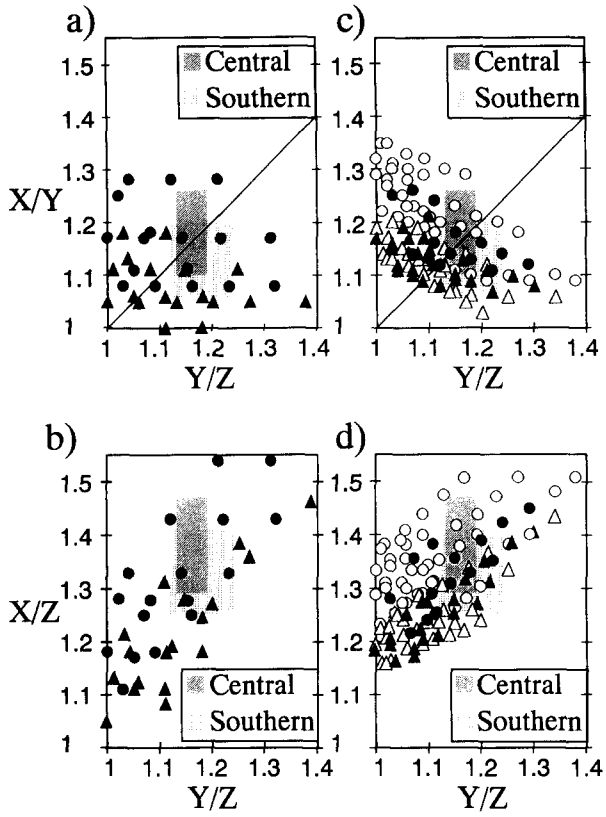

Fig. 5. (a) *X/Y*, *Y/Z* Flinn plot showing the results of the simple two-step simulations. Circles are simulations with LPS by axial symmetric flattening; triangles are simulations with plane strain LPS. (b) *X/Z*, *Y/Z* plot showing the results of the simple two-step simulations; symbology is as in (a). (c) *X/Z*, *Y/Z* Flinn plot showing the results of simulations with triaxial compaction for the central and southern Appalachians. Circles are simulations with LPS by axial symmetric flattening and triangles are simulations with plane strain LPS. Open symbols represent simulations for the central Appalachians, filled symbols represent simulations for the southern Appalachians. (d) *X/Z*, *Y/Z* plot showing the results of simulations with triaxial compaction; symbology is as in (b). The shaded boxes in each plot show the range of admissible solutions for the southern and central regions based on one standard deviation from the average *X/Y*, *X/Z* and *Y/Z* values for each region.

favoring grain dissolution, than silica-cemented sandstones (Gallagher *et al.* 1974) because the aggregates have less grain-contact area to distribute the load; (2) quartz sand aggregates are weaker by an order of magnitude than silica-cemented sandstones (Wilhemi & Somerton 1967, Voight & St. Pierre 1974) for the low temperatures typical of the area during deformation (<200°C, Epstein *et al.* 1977, Harris 1979, Lewis & Hower 1990); and (3) the N–S horizontal shortening during compaction may in fact represent earliest Alleghanian LPS. This LPS would have developed well beyond the limits of foreland thrusting, but within the limits of the orogenic stress domain (Craddock & van der Pluijm 1989). It should be noted that the total displacement from thrusting in the southern Appalachians is a deformation that greatly exceeds the magnitude of this early non-coaxial horizontal shortening.

The simulations predict 10% LPS in the central Appalachians, and a 5% LPS in the southern Appalachians. This result is consistent with greater abundance of intragranular microstructures in the central Appalachians (Onasch & Dunne 1993) and with the samples from there being located in the roof sequence above a blind thrust system. In that position, the sandstone records a greater LPS because it must accommodate shortening from the displacements of the underlying thrust system (Dunne & Ferrill 1988).

Three-dimensional simulations and the transition zone

The transition zone was buried to lithification depths during Acadian molasse sedimentation (Colton 1970, Meckel 1970) like the central Appalachians. Thus, strain factorizations for this region should include the possibility of E–W horizontal shortening during compaction. This region was subjected to first southern and then to central Alleghanian deformation events (Rodgers 1970, Geiser & Engelder 1983, Dean *et al.* 1988). Consequently, factorizations should include the possibility of both southern and central tectonic shortening. These sequential deformations are non-coaxial, which is further enhanced by central Appalachian shortening being superimposed on bedding inclined by the formation of older southern Appalachian macrostructures. Also, the strain increments for simulating deformation in the transition zone are oblique to regional strike (050°), and are not parallel to the local co-ordinate system.

As with the comparison of data to previous simulations, samples were selected from SE-dipping domains that did not contain micro- and mesostructures related to later tectonic events. Four of the six possible samples (white asterices in the transition zone, Fig. 1) had *Z*-axes subnormal to bedding (see Appendix 1). Based on the previous successful simulations, the sequence of events to be modeled is: (1) 30–35% compaction with 3–7% E–W horizontal shortening; (2) 5% LPS by plane strain and axial symmetric flattening along a southern 150° trend; (3) rigid-body rotation to a 25° southeasterly dip, which is within 2° of the inclination for all test stations; and (4) 10% horizontal shortening by plane strain and axial symmetric flattening along a central 120° trend. The 16 permutations that include all events yield calculated finite strain ellipsoids with *X*-axis trends at least 10° outside the allowable range of 040–050° (Fig. 3 and Table 2).

Because these simulations do not yield correct results, one or more of the events must have had a different behavior in the transition zone. The timing of burial is well constrained from the stratigraphic record. Besides, decreasing the syn-compactional horizontal shortening as a function of increasing distance from Acadian compression only increases this mismatch between calculated and actual axial trends. Also, the 5% LPS recorded in the southern Appalachians preceded the development of southern macrostructures, and should be present in the transition, where southern structures such as the Saltville and Narrows thrusts are present (Rodgers 1970). These structures have trends rotated from 060° to 050° by superimposed central Appalachian defor-

Table 3. Admissible simulations with triaxial sedimentary compaction

Region	Compaction (%)	Horizontal volume loss (%)	LPS*	X/Y	Y/Z	X/Z	X axis trend (°)
	30	3	10% a.f.	1.19	1.16	1.38	026
Central	35	7	10% a.f.	1.23	1.15	1.41	021
	35	3.5	10% p.s.	1.14	1.17	1.33	023
	30	4.5	5% a.f.	1.11	1.22	1.35	071
	30	6	5% a.f.	1.13	1.18	1.33	073
	30	7.5	5% a.f.	1.14	1.14	1.31	075
	35	8.75	5% a.f.	1.16	1.20	1.39	076
Southern	35	10.5	5% a.f.	1.18	1.15	1.36	078
	30	3	5% p.s.	1.07	1.22	1.31	071
	30	4.5	5% p.s.	1.09	1.18	1.29	074
	30	6	5% p.s.	1.10	1.15	1.27	077
	35	7	5% p.s.	1.11	1.21	1.35	078
	35	8.75	5% p.s.	1.13	1.17	1.32	079

*a.f.—LPS by axial symmetric flattening; p.s.—LPS by plane strain.

mation. In contrast, the transition does not contain macrostructures of central or modified central Appalachian trend (Rodgers 1970, Dean *et al.* 1988). The central Appalachian deformation operated in the transition without initiating macrostructures and was active at the limits of its deformation domain. As a result, a lesser magnitude and/or more southern orientation for the central LPS could be expected in the transition. These three permutations of magnitude and orientation were included in 48 additional simulations of the compactional and tectonic shortening history in the transition.

Only one of the 16 simulations where just the strain magnitude was reduced to 5% yielded calculated X-axes with the correct trend range. Three of the 32 simulations where the shortening direction was changed by 10° from 120° to 130° with magnitudes of either 5 or 10% yielded orientations and axial ratios equivalent to measured values (Table 2). All successful simulations include 30% compaction with 3.5% horizontal shortening and a 5% southern LPS by axial symmetric flattening. The central shortening event may be either 10% by axial symmetric flattening, or 5% by plane strain or axial symmetric flattening. The deformation paths for the admissible simulations (Fig. 6c) have the first two increments (compaction and southern LPS) that are the same. Again, the paths move to the right and lift off the Y/Z axis during pre-tectonic compaction, and the tectonic shortening events move the paths into the true constrictional field. In summary, the results of strain factorization indicate that the component of central Appalachian shortening in the transition zone was weakly non-coaxial to the main deformation direction in the central Appalachians and may have been of lesser magnitude.

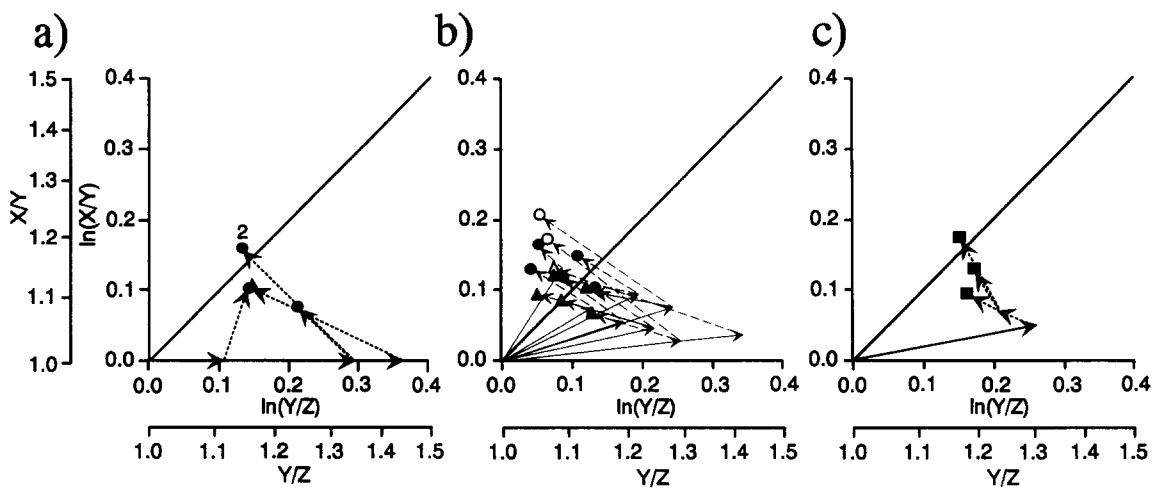

Fig. 6. (a) Logarithmic Flinn plot of five admissible simple two-step simulation deformation paths. Circles are simulations with LPS by axial symmetric flattening and triangles are simulations with LPS by plane strain. 2 locates a simulation that is admissible for both the southern and central Appalachians. (b) Logarithmic Flinn plot of 13 deformation paths for admissible simulations with triaxial sedimentary compaction. Circles are simulations with LPS by axial symmetric flattening and triangles are simulations with LPS by plane strain. Open symbols are for the central Appalachians and filled symbols are for the southern Appalachians. (c) Logarithmic Flinn plot of four admissible transition region simulation deformation paths. In all the graphs, solid lines represent syn-lithification increments and dashed lines represent post-lithification tectonic increments.

SUMMARY

Assumptions

(1) Original porosity in the Tuscarora Sandstone before lithification was approximately 40%.

(2) Porosity that was not chemically preserved as silica cement was physically destroyed by grain-boundary sliding, grain cataclasis and grain solution. This porosity reduction is a volume loss.

(3) Because tectonic LPS is commonly transport-parallel, compaction during lithification had a non-coaxial horizontal volume-loss component that caused the finite strain ellipsoid axes to be oblique to strike and dip.

Constraints

(1) Diagenetic cement constitutes about 10 ± 5% of the Tuscarora Sandstone and admissible models must reduce original porosity to this value.

(2) Both detrital quartz grains and silica-cement are deformed by intragranular microstructures, indicating a post-lithification LPS event with microstructural abundance as an indicator of relative strain intensity.

(3) No microstructural evidence such as bed-normal stylolites exists for post-compactional tectonic pressure solution, so tectonic LPS in the lithified Tuscarora sandstone was volume-constant.

(4) Microstructural suites (Onasch & Dunne 1993) indicate that samples used in this study from both SE-dipping flats or macro-anticline limbs underwent only diagenetic compaction and tectonic LPS.

(5) Calculated strains from simulations must lie within 1 SD of mean X/Y, Y/Z and X/Z ratios, within 5° of average X-axis trends for each region and yield a subvertical Z axis to be admissible.

Results

(1) Three-dimensional factorization for Tuscarora Sandstone samples with finite strains due to compaction and LPS indicate: in the southern Appalachians, 30% compaction including 4.5–7.5% N–S horizontal shortening, or 35% compaction including 7–9% N–S horizontal shortening, was followed by 5% LPS by plane strain or axial symmetric shortening. In the central Appalachians, 30% compaction including 3% E–W horizontal shortening, or 35% compaction including 3.5–7% E–W horizontal shortening, was followed by 10% LPS by plane strain or axial symmetric flattening.

(2) In the transition zone, where central tectonic shortening overprints southern LPS and macrostructures, the factorization results indicate a deformation sequence of: (a) 30% compaction with 3% E–W horizontal shortening similar to the central Appalachians; (b) 5% LPS by axial symmetric flattening during deformation of southern affinity; (c) a rigid-body rotation of 25° around strike from emplacement above ramps related to southern Appalachian thrusting; and (d) a central Appalachian shortening at the limits of that deformation domain with a shortening direction rotated to 130° from the normal 120° and magnitude probably reduced from 10 to 5%.

(3) Finite strains in the Tuscarora Sandstone are dominated by compaction. This compaction, however, is not symmetric in the plane of bedding and includes a component of E–W shortening in the central Appalachians and N–S shortening in the southern Appalachians by porosity reduction. Horizontal shortening during the compaction event in the southern Appalachians is greater than later Alleghanian LPS, perhaps indicating the importance of a very early pre-thrusting shortening in unlithified sand.

(4) Plane strain is not necessitated during LPS and, in fact, axial symmetric flattening more commonly yielded successful modeling results.

Acknowledgements—This work was funded by NSF grant EAR-8915949 to Dunne and Onasch, and grants from the Geological Society of America, the American Association of Petroleum Geologists, Sigma Xi, and Shell Oil Company to Couzens. The generosity of Art Schultz and Jerry Bartholomew, who shared data from maps in press, is greatly appreciated. Maria Leary is thanked for her assistance in fieldwork. Discussions with Dr Richard Williams about the mathematics involved were very helpful and appreciated. The manuscript was significantly improved by the comments of Mary Ford, Gautam Mitra, David Gray and an anonymous reviewer. This work represents a portion of the requirements for Couzens' and Glass' masters theses.

REFERENCES

Anton, H. 1984. *Elementary Linear Algebra*. Wiley, New York.

Bartholomew, M. J. 1987. Structural evolution of the Pulaski thrust system, southwestern Virginia. *Bull. geol. Soc. Am.* **99**, 491–510.

Beard, D. C. & Weyl, P. K. 1973. Influence of texture on porosity and permeability of unconsolidated sand. *Bull. Am. Ass. Petrol. Geol.* **57**, 349–369.

Berger, P., Perry, W. J., Jr. & Wheeler, R. L. 1979. Three stage model of brittle deformation in the central Appalachians. *Southeastern Geol.* **20**, 59–67.

Boas, M. L. 1983. *Mathematical Methods in the Physical Sciences*. Wiley, New York.

Cobbold, P. R. 1979. Removal of finite deformation using strain trajectories. *J. Struct. Geol.* **1**, 67–72.

Colton, G. W. 1970. The Appalachian basin—Its depositional sequences and their geologic relationships. In: *Studies of Appalachian Geology: Central and Southern* (edited by Fisher, G. W., Pettijohn, F. J., Read, J. C., Jr. & Weaver, K. N.). Wiley-Interscience, New York, 5–47.

Cotter, E. 1988. Hierarchy of sea-level cycles in the medial Silurian siliciclastic succession of Pennsylvania. *Geology* **16**, 242–245.

Craddock, J. P. & van der Pluijm, B. A. 1989. Late Paleozoic deformation of the cratonic carbonate cover of eastern North America. *Geology* **17**, 416–419.

Dean, S. L., Kulander, B. R. & Skinner, J. M. 1988. Structural chronology of the Alleghanian orogeny in southeastern West Virginia. *Bull. geol. Soc. Am.* **100**, 299–310.

Dennison, J. 1970. Silurian stratigraphy and sedimentary tectonics of southern West Virginia and adjacent Virginia. In: *Silurian Stratigraphy, Central Appalachian Basin*. Appalachian Geological Society, Charleston, West Virginia, 2–33.

Dunne, W. M. 1986. Mesostructural development in detachment folds: an example from West Virginia. *J. Geol.* **94**, 473–488.

Dunne, W. M. & Ferrill, D. A. 1988. Blind thrust systems. *Geology* **16**, 33–36.

Dunne, W. M., Onasch, C. M. & Williams, R. 1990. The problem of

strain-marker centers and the Fry method. *J. Struct. Geol.* **12**, 933–938.

Elias, B. P. & Hajash, A., Jr. 1992. Changes in quartz solubility and porosity due to effective stress: An experimental investigation of pressure solution. *Geology* **20**, 451–454.

Engelder, T. & Geiser, P. A. 1979. The relationship between pencil cleavage and lateral shortening within the Devonian section of the Appalachian Plateau, New York. *Geology* **7**, 460–464.

Epstein, A. G., Epstein, J. B. & Harris, L. D. 1977. Conodont color alteration—an index to organic metamorphism. *Prof. Pap. U.S. geol. Surv.* **995**.

Erslev, E. A. 1988. Normalized center-to-center strain analysis of packed aggregates. *J. Struct. Geol.* **10**, 201–209.

Evans, M. A. & Dunne, W. M. 1991. Strain factorization and partitioning in a foreland thrust sheet. *J. Struct. Geol.* **13**, 13–25.

Ferrill, B. & Thomas, W. A. 1988. Acadian dextral transpression and synorogenic sedimentary successions in the Appalachians. *Geology* **16**, 604–608.

Fry, N. 1979. Random point distributions and strain measurement in rocks. *Tectonophysics* **60**, 89–105.

Gallagher, J. J., Jr., Friedman, M., Handin, J. & Sowers, G. M. 1974. Experimental studies relating to microfracture in sandstone. *Tectonophysics* **21**, 203–247.

Geiser, P. A. 1988. Mechanisms of thrust propagation: some examples and implications from the analysis of overthrust terranes. *J. Struct. Geol.* **10**, 829–845.

Geiser, P. A. & Engelder, T. 1983. The distribution of layer parallel shortening fabrics in the Appalachian foreland of New York and Pennsylvania; Evidence for two non-coaxial phases of the Alleghanian orogeny. In: *Contributions to the Tectonics and Geophysics of Mountain Chains* (edited by Hatcher, R. D., Williams, H. & Zeitz, I.). *Mem. geol. Soc. Am.* **158**, 161–175.

Gendzwill, D. J. & Stauffer, M. R. 1981. Analysis of triaxial ellipsoids: their shapes, plane sections and plane projections. *Math. Geol.* **13**, 135–152.

Gray, D. R. & Willman, C. E. 1991. Thrust-related strain gradients and thrusting mechanisms in a chevron-folded sequence, southeastern Australia. *J. Struct. Geol.* **13**, 691–710.

Groshong, R. H., Jr. 1972. Strain calculated from twinning in calcite. *Bull. geol. Soc. Am.* **83**, 2025–2038.

Groshong, R. H., Jr. 1988. Low-temperature deformation mechanisms and their interpretation. *Bull. geol. Soc. Am.* **100**, 1329–1360.

Harris, A. G. 1979. Conodont color alteration, an organo-mineral metamorphic index, and its application to Appalachian Basin geology. In: *Aspects of Diagenesis* (edited by Scholle, P. A. & Schluger, P. R.). *Spec. Publ. Soc. econ. Paleont. Miner.* **26**, 3–16.

Hatcher, R. D., Jr., Thomas, W. A., Geiser, P. A., Snoke, A. W., Mosher, S. & Wiltschko, D. V. 1989. Alleghanian orogen. In: *The Appalachian–Ouachita Orogen in the United States* (edited by Hatcher, R. D., Jr., Thomas, W. A. & Viele, G. W.). *Geol. Soc. Am., The Geology of North America* **F-2**, 223–318.

Hayes, A. W. 1974. Origin of the Tuscarora Formation (Lower Silurian), southwestern Virginia. Unpublished Ph.D. dissertation, Virginia Polytechnic Institute and State University.

Heald, M. T. 1955. Stylolites in sandstones. *J. Geol.* **63**, 101–114.

Heald, M. T. 1956. Cementation of Simpson and St. Peter sandstones in parts of Oklahoma, Arkansas, and Missouri. *J. Geol.* **64**, 16–30.

Hobbs, B. E., Means, W. D. & Williams, P. F. 1976. *An Outline of Structural Geology*. Wiley, New York.

Hossack, J. R. 1979. The correction of stratigraphic sections for tectonic finite strains in the Bygdin area, Norway. *J. geol. Soc. Lond.* **135**, 229–241.

Houseknecht, D. W. 1987. Assessing the relative importance of compaction processes and cementation to reduction of porosity in sandstones. *Bull. Am. Ass. Petrol. Geol.* **71**, 633–642.

Houseknecht, D. W. 1988. Intergranular pressure solution in four quartzose sandstones: *J. sedim. Petrol.* **58**, 228–246.

Kamb, W. B. 1959. Ice petrofabric observations from Blue Glacier, Washington, in relation to theory and experiment. *J. geophys. Res.* **57**, 153–170.

Kligfield, R., Crespi, J., Naruk, S. & Davis, G. H. 1984. Displacement and strain patterns of extensional orogens. *Tectonics* **3**, 577–609.

Kreisa, R. D. & Springer, D. A. 1987. Lithostratigraphy and biostratigraphy of the Martinsburg Formation in southwestern Virginia, with descriptive sections. In: *Contributions to Virginia Geology—V. Virginia Div. Miner. Resourc. Publ.* **74**, 33–54.

Lewis, S. E. & Hower, J. C. 1990. Implications of thermal events on thrust emplacement sequence in the Appalachian fold and thrust belt: some new vitrinite reflectance data. *J. Geol.* **98**, 927–942.

Marshak, S. & Engelder, T. 1985. Development of cleavage in limestones of a fold-thrust belt in eastern New York. *J. Struct Geol.* **7**, 345–359.

Means, W. D. 1976. *Stress and Strain: Basic Concepts of Continuum Mechanics for Geologists*. Springer, New York.

Meckel, L. D. 1970. Paleozoic alluvial deposition in the central Appalachians: A summary. In: *Studies of Appalachian Geology: Central and Southern* (edited by Fisher, G. W., Pettijohn, F. J., Read, J. C., Jr. & Weaver, K. N.). Wiley-Interscience, New York, 49–67.

Mitra, G. & Yonkee, W. A. 1985. Relationship of spaced cleavage to folds and thrusts in the Idaho–Utah–Wyoming thrust belt. *J. Struct. Geol.* **7**, 361–377.

Mitra, S. & Beard, W. C. 1980. Theoretical models of porosity reduction by pressure solution for well-sorted sandstones. *J. sedim. Petrol.* **50**, 1347–1360.

Narr, W. & Currie, J. B. 1982. Origin of fracture porosity—example from Altamont Field, Utah. *Bull. Am. Ass. Petrol. Geol.* **66**, 1231–1247.

Nickelsen, R. P. 1979. Sequence of structural stages of the Alleghany orogeny at the Bear Valley strip mine, Shamokin, Pennsylvania. *Am. J. Sci.* **279**, 225–271.

Onasch, C. M. 1990. Microfractures and their role in deformation of a quartz arenite from the central Appalachian foreland. *J. Struct. Geol.* **12**, 883–894.

Onasch, C. M. & Dunne, W. M. 1993. Variation in quartz arenite deformation mechanisms between a roof sequence and duplexes. *J. Struct. Geol.* **15**, 465–475.

Pryor, W. A. 1973. Permeability–porosity patterns and variations in some Holocene sand bodies. *Bull. Am. Ass. Petrol. Geol.* **57**, 162–189.

Protzman, G. M. & Mitra, G. 1990. Strain fabric associated with the Meade thrust sheet: implications for cross-section balancing. *J. Struct. Geol.* **12**, 403–417.

Rader, E. K. & Heinika, W. S. 1978. Ordovician shelf to basin transition. Shenandoah Valley, Virginia. In: *Contributions to Virginia Geology—III. Virginia Div. Miner. Resource. Publ.* **11**, 32–34.

Ramsay, J. G. 1967. *Folding and Fracturing of Rocks*. McGraw-Hill, New York.

Ramsay, J. G. & Huber, M. I. 1983. *The Techniques of Modern Structural Geology, Volume* 1: *Strain Analysis*. Academic Press, New York.

Ramsay, J. G. & Huber, M. I. 1987. *The Techniques of Modern Structural Geology, Volume* 2: *Folds and Fractures*. Academic Press, New York.

Ramsay, J. G. & Wood, D. S. 1973. The geometric effects of volume change during deformation processes. *Tectonophysics* **13**, 263–277.

Reks, I. J. & Gray, D. R. 1983. Strain patterns and shortening in a folded thrust sheet: an example from the southern Appalachians. *Tectonophysics* **93**, 99–128.

Rodgers, J. 1970. *The Tectonics of the Appalachians*. John Wiley & Sons, New York.

Rutter, E. H. 1976. Kinetics of rock deformation by pressure solution. *Phil. Trans. R. Soc. Lond.* **A283**, 203–219.

Sibley, D. F. & Blatt, H. 1976. Intragranular pressure solution and cementation of the Tuscarora orthoquartzite. *J. sedim. Petrol* **46**, 881–896.

Simon, R. I. & Gray, D. R. 1982. Interrelations of mesoscopic structures and strain across a small regional fold, Virginia Appalachians. *J. Struct. Geol.* **4**, 271–289.

Stephenson, L. P., Plumley, W. J. & Palciauskas, V. V. 1991. A model for sandstone compaction by grain interpenetration. *J. sedim. Petrol.* **62**, 11–22.

Voight, B. & St. Pierre, B. H. P. 1974. Stress history and rock stress. *Proc. 3rd Rock Mech. Congr. ISRM* **2**, 580–582.

Whisonant, R. C. 1977. Lower Silurian Tuscarora (Clinch) dispersal patterns in western Virginia. *Bull. geol. Soc. Am.* **88**, 215–220.

Wilhemi, B. & Somerton, W. H. 1967. Simultaneous measurement of pore and elastic properties of rocks under triaxial conditions. *J. Soc. Petrol. Engng (AIME)* **7**, 283–294.

Woodward, N. B., Gray, D. R. & Spears, D. B. 1986. Including strain in balanced cross-sections. *J. Struct. Geol.* **8**, 313–324.

Zoback, M. L. & Zoback, M. D. 1990. Tectonic stress field of the continental United States. In: *Geophysical Framework of the Continental United States* (edited by Pakiser, L. & Mooney, W.). *Mem. geol. Soc. Am.* **172**.

APPENDIX 1

Bedding dips at sample locations with orientations and magnitudes of strain ellipsoids for bedding restored to the horizontal

Sample	Bedding dip*	*X*-trend	*X*-plunge	*Y*-trend	*Y*-plunge	*Z*-trend	*Z*-plunge	*X/Y*	*Y/Z*	*X/Z*	Structure†	Region‡
A-1	350/37NE(OT)	290	33	180	28	59	44	1.19	1.09	1.30	1	C
BG-1	028/36SE(OT)	245	28	149	12	38	59	1.21	1.23	1.49	1	C
BG-2	012/35SE(OT)	206	16	298	8	54	72	1.18	1.14	1.35	1	C
A-5	023/89SE(OT)	94	29	186	4	284	61	1.06	1.27	1.34	3	C
A-6	050/60NW	76	28	331	26	205	50	1.09	1.06	1.16	3	C
A-9	030/54SE(OT)	121	14	27	19	245	66	1.18	1.19	1.41	3	C
B-4	011/55NW	266	29	0	7	103	60	1.17	1.17	1.37	3	C
B-7	044/78NW	353	20	253	24	119	58	1.08	1.04	1.12	3	C
B-11	046/69NW	280	28	10	1	103	62	1.13	1.09	1.23	3	C
MM-1	068/67NW	220	10	123	35	323	53	1.27	1.16	1.47	3	C
A-4	035/60SE	2	6	99	46	266	43	1.08	1.22	1.32	4	C
A-8	052/28SE	320	37	55	6	153	52	1.21	1.13	1.37	4	C
B-5	020/59NW	338	38	73	6	170	51	1.06	1.09	1.15	4	C
B-6	040/53SE	321	37	330	11	73	51	1.15	1.29	1.48	4	C
B-8	015/28SE	58	24	167	36	302	44	1.15	1.09	1.25	4	C
B-9	025/31SE	201	30	104	12	356	57	1.23	1.20	1.47	4	C
B-10	020/14SE	185	39	94	2	2	51	1.12	1.13	1.26	4	C
MM-2	024/35SE	12	34	103	2	196	56	1.11	1.18	1.31	4	C
B-1	050/08NW	5	7	267	49	101	40	1.08	1.32	1.43	5	C
B-2	045/10SE	183	27	283	19	45	56	1.30	1.15	1.50	5	C
B-3	045/10NW	220	11	314	22	106	65	1.14	1.18	1.34	5	C
A-2	018/15NW	178	11	87	1	354	79	1.16	1.11	1.29	6	C
A-3	018/15NW	175	24	79	12	324	63	1.29	1.11	1.43	6	C
A-7	315/6NE	184	30	93	1	2	60	1.16	1.18	1.37	6	C
C-1	060/60SE(OT)	119	9	216	37	17	52	1.17	1.03	1.21	1	T
C-2	042/70SE(OT)	355	8	90	28	250	60	1.18	1.14	1.34	1	T
D-10	037/56SE(OT)	218	3	308	2	64	86	1.04	1.36	1.42	1	T
E-1	047/50SE(OT)	205	5	115	0	25	85	1.20	1.27	1.52	1	T
E-4	055/36SE	249	3	159	5	9	84	1.16	1.23	1.43	2	T
C-4	050/57NW	108	24	230	50	3	29	1.06	1.02	1.08	3	T
C-6	058/58SE(OT)	38	1	308	4	141	86	1.12	1.10	1.23	3	T
C-7	275/44SW	228	27	335	30	104	47	1.30	1.14	1.48	3	T
D-2a	053/80SE(OT)	24	8	289	30	128	59	1.06	1.28	1.36	3	T
D-2b	063/74SE(OT)	247	42	333	7	71	47	1.28	1.15	1.47	3	T
E-6	035/58SE(OT)	184	4	92	24	282	66	1.18	1.25	1.47	3	T
SC-3	060/50SE(OT)	117	1	27	4	215	86	1.02	1.20	1.22	3	T
C-3	015/63SE	14	32	110	9	213	56	1.30	1.11	1.44	4	T
D-6a	080/21SE	52	6	322	3	208	84	1.02	1.26	1.28	4	T
D-6b	069/12SE	286	3	185	73	17	16	1.41	1.06	1.49	4	T
E-5	066/24SE	261	2	351	3	147	86	1.22	1.17	1.43	4	T
E-7	045/29SE	236	24	145	3	48	66	1.08	1.18	1.27	4	T
SC-4	060/23SE	70	1	160	3	325	87	1.16	1.16	1.34	4	T
SC-6	060/26SE	58	22	148	1	242	68	1.04	1.26	1.31	4	T
D-1	055/31SE	252	14	144	52	352	34	1.15	1.15	1.32	5	T
D-9	055/33SE	275	12	25	39	171	48	1.25	1.17	1.46	5	T
E-8	025/15SE	51	23	315	14	196	63	1.14	1.12	1.28	5	T
C-5	045/23SE	225	40	135	1	44	50	1.10	1.10	1.21	6	T
C-8	340/05SW	291	9	147	79	22	6	1.10	1.21	1.33	6	T
C-9	325/10SW	39	35	143	20	257	48	1.15	1.10	1.27	6	T
D-5	056/48SE	202	19	105	19	333	63	1.17	1.21	1.42	6	T
D-7	067/08SE	270	37	171	12	66	51	1.01	1.18	1.19	6	T
D-8	010/23E	175	7	266	3	17	83	1.14	1.32	1.50	6	T
WS-1	055/20SE	62	38	153	1	243	52	1.18	1.15	1.36	6	T
WS-2	090/12S	43	1	134	13	309	77	1.16	1.17	1.36	6	T
D-3	030/20SE	250	11	343	15	125	72	1.07	1.27	1.36		T
D-4	085/67N	93	20	243	27	325	55	1.10	1.22	1.34		T
F-4	068/56SE(OT)	22	0	292	8	113	82	1.08	1.19	1.29	1	S
H-1	084/75SE(OT)	83	1	173	2	329	88	1.05	1.33	1.39	1	S
H-6b	080/25SE	145	14	236	6	348	75	1.02	1.33	1.36	1	S
F-3	083/39SE	106	16	12	15	241	68	1.10	1.17	1.29	2	S
F-5a	082/25SE	287	7	19	16	174	72	1.05	1.19	1.25	2	S
F-5	089/25SE	17	15	109	9	128	73	1.12	1.21	1.36		S
F-6	070/43SE	272	4	2	12	165	77	1.13	1.14	1.29	2	S
H-3	102/38SE(OT)	286	15	191	19	52	66	1.18	1.11	1.31	2	S
SC-1	055/90	233	26	324	0	54	64	1.09	1.21	1.32	3	S
F-1	074/30SE	292	22	42	40	180	42	1.12	1.20	1.34	5	S
F-2	069/20SE	259	35	159	14	50	51	1.15	1.06	1.22	5	S
F-15	058/49SE	70	20	167	19	297	62	1.09	1.25	1.36	5	S
H-2	078/42SE	355	15	90	18	226	66	1.09	1.13	1.23	5	S
H-4	063/19SE	194	12	97	28	305	59	1.26	1.43	1.80	5	S
H-5	090/33SE	234	48	21	37	124	17	1.13	1.09	1.23	5	S
H-6a	044/31SE	166	22	256	1	340	68	1.12	1.38	1.15	5	S
SC-2	159/06NE	74	22	173	21	302	59	1.19	1.15	1.37	6	S

Continued

Continued

Sample	*Bedding dip**	*X*-trend	*X*-plunge	*Y*-trend	*Y*-plunge	*Z*-trend	*Z*-plunge	*X/Y*	*Y/Z*	*X/Z*	Structure†	Region‡
F7C	138/06NE	118	14	209	2	308	76	1.22	1.15	1.40		S
F8C	177/06W	259	8	169	0	78	82	1.06	1.40	1.48		S
F9C	144/11NW	95	6	187	25	352	64	1.38	1.14	1.57		S
F10C	112/05SE	36	17	127	1	197	73	1.15	1.21	1.39		S
F11C	112/10SE	330	14	64	18	203	67	1.35	1.06	1.43		S
F13C	097/31N	264	10	171	17	25	70	1.05	1.23	1.29		S

*OT—overturned.
†1—footwall ramp; 2—hangingwall ramp; 3—northwest anticlinal limbs; 4—southeast anticlinal limbs; 5—hangingwall flats; 6—anticlinal hinges.
‡C—central; T—transition; S—southern.

APPENDIX 2

DETERMINATION OF STRAIN ELLIPSOID MAGNITUDE AND ORIENTATION

Once a deformation matrix, D, has been calculated, a strain ellipsoid is determined by using D to deform a unit sphere. The resulting strain ellipsoid may be represented in the form of an origin-centered quadratic surface:

$$ax^2 + by^2 + cz^2 + 2lxy + 2mxz + 2nyz = 1, \quad \text{(A1)}$$

which in matrix form is:

$$[x\ y\ z]\begin{bmatrix} a & l & m \\ l & b & n \\ m & n & c \end{bmatrix}\begin{bmatrix} x \\ y \\ z \end{bmatrix} = 1 \quad \text{(A2)}$$

(where the 3 × 3 matrix is the matrix of coefficients). The coefficients for the equation of the unit sphere:

$$x^2 + y^2 + z^2 = 1 \quad \text{(A3)}$$

may be represented by the identity matrix:

$$I = \begin{bmatrix} 1 & 0 & 0 \\ 0 & 1 & 0 \\ 0 & 0 & 1 \end{bmatrix} = 1. \quad \text{(A4)}$$

The deformation matrix D, can be used to deform a sphere, I, by the following relationship (Boas 1983):

$$Q = D^{-1}I(D^{-1})_t = D^{-1}(D^{-1})_t, \quad \text{(A5)}$$

where Q, in the form of the matrix of coefficients (equation A2), is the strain ellipsoid resulting from the deformations, D.

The axial lengths of the strain ellipsoid and their orientations may be determined from the eigenvalues and eigenvectors of Q, respectively. A vector, $\bar{s}$, is an eigenvector of Q if: $Q\bar{s}$ is a scalar multiple of $\bar{s}$ (equation A6) (Anton 1984),

$$Q\bar{s} = \mu\bar{s}, \quad \text{(A6)}$$

where μ is the eigenvalue corresponding to $\bar{s}$. The eigenvector condition in matrix notation is:

$$\begin{bmatrix} a & l & m \\ l & b & n \\ m & n & c \end{bmatrix}\begin{bmatrix} x \\ y \\ z \end{bmatrix} = \mu\begin{bmatrix} x \\ y \\ z \end{bmatrix} \text{ yielding } \begin{bmatrix} a-\mu & l & m \\ l & b-\mu & n \\ m & n & c-\mu \end{bmatrix}\begin{bmatrix} x \\ y \\ z \end{bmatrix} = 0. \quad \text{(A7)}$$

Solving this set of equations, we will get the trivial solution, $x = y = z = 0$, unless the determinant of the system of equations is equal to zero (equation A8).

$$\begin{vmatrix} a-\mu & l & m \\ l & b-\mu & n \\ m & n & c-\mu \end{vmatrix} = 0. \quad \text{(A8)}$$

Solving the determinant (equation A8) yields a cubic equation in terms of μ. The three roots of this cubic equation are the eigenvalues: μ_1, μ_2 and μ_3, which represent the lengths of the principal axes of the strain ellipsoid. Relative to the principal axes (X,Y,Z) the equation of the strain ellipsoid can be represented as:

$$[X\ Y\ Z]\begin{bmatrix} \mu_1 & 0 & 0 \\ 0 & \mu_2 & 0 \\ 0 & 0 & \mu_3 \end{bmatrix}\begin{bmatrix} X \\ Y \\ Z \end{bmatrix} = 1 \quad \text{(A9)}$$

$$\mu_1 X^2 + \mu_2 Y^2 + \mu_3 Z^2 = 1. \quad \text{(A10)}$$

From equation (A10), the lengths of the axes are:

$$\frac{1}{\sqrt{\mu_1}}, \frac{1}{\sqrt{\mu_2}}, \frac{1}{\sqrt{\mu_3}}.$$

Three eigenvectors $(\bar{s}_1, \bar{s}_2, \bar{s}_3)$ (equation A6), one for each principal axis, are then determined by substituting μ_1, μ_2 and μ_3 into equation (A7) and solving for x, y and z. The direction of each eigenvector is the direction of a principal axis that was determined in real space (x = dip-direction, y = strike direction, z = vertical) by: (1) normalizing the vector to consider only its down-plunge direction; (2) determination of the angle, β, from the plunge direction to the dip-direction (x) using the following relationship:

$$\cos\beta = \frac{x}{\sqrt{(x^2 + y^2)}} \quad \text{(A11)}$$

and; (3) determination of an azimuthal direction by picking a sign convention where positive x (dip-direction) is southeast, and positive y (strike) is southwest. If $x > 0$ and $y > 0$, β was added to the dip-direction. If $x > 0$ and $y < 0$, β was subtracted from the dip-direction, if $x < 0$ and $y > 0$, β was subtracted from the dip-direction + 180°. Or if $x < 0$ and $y < 0$, β was added to the dip-direction + 180°.